A satellite-based estimate of aerosol-cloud microphysical effects over the Arctic Ocean

Lauren M. Zamora[1,2], Ralph A. Kahn[2], Klaus B. Huebert[3], Andreas Stohl[4], Sabine Eckhardt[4]

[1]Earth System Science Interdisciplinary Center, University of Maryland, College Park, MD, USA
5   [2]NASA Goddard Space Flight Center, Greenbelt, MD, USA
[3]Horn Point Laboratory, University of Maryland Center for Environmental Science, Cambridge, MD, USA
[4]NILU – Norwegian Institute for Air Research, Kjeller, Norway

Correspondence to: Lauren M. Zamora (lauren.m.zamora@nasa.gov)

Abstract. Climate predictions for the rapidly changing Arctic are highly uncertain, largely due to a poor understanding of

10   the processes driving cloud properties. In particular, cloud fraction (CF) and cloud phase (CP) have major impacts on energy budgets, but are poorly represented in most models, often because of uncertainties in aerosol-cloud interactions. Here we use over 10 million satellite observations coupled with aerosol transport model simulations to quantify regional-scale microphysical effects of aerosols on CF and CP over the Arctic Ocean during polar night, when direct and semi-direct aerosol effects are minimal. Combustion aerosols over sea ice are associated with very large (~25 W m^{-2}) differences in

15   longwave cloud radiative effects at the sea ice surface. However, co-varying meteorological changes on factors such as CF likely explain much of this signal - for example, explaining up to 91% of the CF differences between the full dataset and the clean-condition subset. After normalizing for meteorological regime, aerosol microphysical effects have small but significant regional-scale impacts on CF, CP, and precipitation frequency. These effects indicate that dominant aerosol-cloud microphysical mechanisms are related to the relative fraction of liquid-containing clouds, with implications for a warming

20   Arctic.

1 Introduction

Cloud cover has a major influence on surface heating, precipitation, and future climate over the Arctic (Boucher et al., 2013), and may play a role in the enhanced warming over the Arctic compared to lower latitude regions (Södergren et al., 2017), known as Arctic amplification. Aerosols can influence a number of factors relevant to cloud fraction, including cloud droplet

25   number, phase, lifetime, and probability of precipitation (Albrecht, 1989; Coopman et al., 2016; Girard et al., 2005; Lance et al., 2011; Lindsey and Fromm, 2008; Zamora et al., 2017). However, the regional-scale importance of aerosol microphysical processes on CF has been difficult to constrain from observations and models. This is mainly due to the complexity of the responses of different types of clouds to different aerosol types and concentrations (Fan et al., 2016; Fu and Xue, 2017; Stevens et al., 2017; Zhao et al., 2018), poorly constrained aerosol concentrations (particularly in winter and beneath thick

30   cloud cover), and confounding effects from co-varying meteorology (Gryspeerdt et al., 2016). These uncertainties contribute

to the large uncertainties in model CF and CP (de Boer et al., 2011; Cesana and Chepfer, 2012; Chernokulsky and Mokhov, 2012; Kay et al., 2010; Liu et al., 2011; Qian et al., 2012; Stanfield et al., 2014; Zib et al., 2012). To account for the impact of meteorological co-variability on Arctic CF, observations covering large spatial and temporal scales are required, making it difficult to estimate the regional importance of aerosol microphysical effects from *in situ* observations alone. These uncertainties have precluded better constraints on the mechanisms by which aerosols affect cloud microphysics (Morrison et al., 2012) and on general model estimates of their overall importance.

Here we provide the first observation-based constraint on regional aerosol microphysical effects on total nighttime CF over the Arctic Ocean within the spectrum of current-day aerosol and meteorological conditions. Estimates of aerosol microphysical effects on operational, satellite-defined CF are obtained from two years of remote sensing data and output from the FLEXPART Lagrangian particle dispersion model (Stohl et al., 1998, 2005). We use the model to provide estimates of how clean or polluted the observed air masses were. We then identify regionally averaged cloud property differences between the full dataset (hereafter referred to as "all conditions") and a subset where combustion aerosols are at clean background levels ("clean conditions"). By comparing clean to all conditions, as opposed to comparing clean to non-clean or polluted-only conditions, our estimates account for the relatively high frequency of clean and low-aerosol conditions, and reflect the true regional microphysical effects of combustion-derived aerosols more accurately. By averaging millions of observations after stratifying them by temperature and relative humidity, we minimize confounding effects of local and regional-scale meteorological co-variability. A major strength of this method, which depends primarily on direct observations, is that it requires no detailed parameterization of the fraction of cloud-active aerosols or underlying microphysical mechanisms to constrain the importance of regional-scale aerosol microphysical effects on Arctic clouds.

2 Methods

Tropospheric cloud data during polar night over the Arctic Ocean were collected from 1 January 2008 to 7 December 2009, between 60 and 82° N and 0.6-8.5 km above sea level. These years had typical moisture fluxes and total cloud fractions compared to other recent years (Boisvert and Stroeve, 2015; Kay and L'Ecuyer, 2013). We focused on observations during polar night (solar zenith angle, SZA, > 90°) mainly to isolate indirect effects of aerosols on clouds as much as possible from confounding direct and semi-direct aerosol radiative effects. The nighttime focus also reduces uncertainties from any residual diurnal changes in cloud fraction, and is associated with a better lidar signal-to-noise ratio (used for aerosol transport model validation, see Supplemental Data). Data from all months meeting the above criteria were included except those between May and July. These were excluded to avoid geographic bias in the analysis, as the few nighttime data that were available during this period tended to occur mainly at the lowest latitudes. Clouds below 0.6 km were not assessed due to near-ground uncertainties in the CloudSat and CALIPSO data (de Boer et al., 2009; Liu et al., 2017).

Oceanic areas were determined by ETOPO1 Bedrock GMT4 data (Amante and Eakins, 2009). Oceanic clouds were separated into open ocean and sea ice regions following Zamora et al. (2017): for each profile, the corresponding monthly fractional sea ice cover was determined from the NOAA/NSIDC Climate Data Record of Passive Microwave Sea Ice Concentration, version 2 (Meier et al., 2013; Peng et al., 2013), and samples associated with > 80% or < 20% monthly sea

5   ice fractions were classified as being over sea ice or open ocean, respectively.

2.1 Aerosol transport model

Passive remote sensors provide no aerosol data at night, and do not provide reliable aerosol data over bright sea ice or under clouds. Active lidar signals often get attenuated in clouds. Moreover, active sensors such as CALIPSO cannot always detect dilute aerosols, even in conditions with the highest lidar sensitivity (i.e., above clouds at night (Zamora et al., 2017)).

10   Therefore, the presence of combustion aerosols for comparison to the satellite cloud data was estimated with vertically-resolved modeled black carbon (BC) aerosol estimates from the FLEXible PARTicle dispersion model (FLEXPART) (Stohl et al., 1998, 2005). Here, FLEXPART was driven with meteorological analysis data from the European Centre for Medium-Range Weather Forecasts (ECMWF) at a resolution of 1˚ longitude and 1˚ latitude. Anthropogenic and biomass burning BC emissions were based on the ECLIPSE (Evaluating the CLimate and Air Quality ImPacts of ShortlivEd Pollutants) (Stohl et

15   al., 2015) and GFED (Global Fire Emission Database) (Giglio et al., 2013) inventories, respectively. Model output was produced in five vertical layers between 0.6-1.5, 1.5-2.5, 2.5-4, 4-6, and 6-8.5 km. Note that the resolution of the meteorological input data is much higher (91 levels) and, as a Lagrangian model, FLEXPART has no discrete resolution for the particle transport. BC emissions were based on the ECLIPSE emission inventory (Stohl et al., 2015). Note that emission fluxes in the model rely on inventories of emission factor measurements that partially include thermooptical measurements,

20   which may not always completely differentiate between BC and "brown" or organic carbon (BrC or OC) (Russell et al., 2014; Samset et al., 2018). Further details on the model and its configuration can be found in Zamora et al. (2017).

FLEXPART is widely used, and is well-validated for the purpose of studying Arctic smoke and pollution transport (Damoah et al., 2004; Eckhardt et al., 2015; Forster et al., 2001; Paris et al., 2009; Sodemann et al., 2011; Stohl et al., 2002, 2003,

25   2015; Zamora et al., 2017). FLEXPART BC is used in this study as a proxy for all combustion aerosols, and the association of high levels of modeled BC with CALIPSO aerosols in general (Zamora et al., 2017) indicates that modeled BC is a fairly good proxy for strong aerosol layers during polar night, even though some local sources of combustion aerosols[6] might not be included in the model. Model comparisons to CALIPSO aerosol data in the study region also indicate that model-identified clean conditions (BC < 30 ng m^{-3}) are associated with significantly lower levels of CALIPSO aerosol layer

30   presence relative to average or polluted conditions (see supplement for further details).

2.2 Cloud remote sensing observations

Cloud fraction is not well defined in the literature. Here, it is operationally defined based on the CloudSat algorithm, in

CloudSat products available at a vertical resolution of 250 m. Cloud base and top heights were originally obtained from the 2B-GEOPROF-lidar product (Mace et al., 2009; Mace and Zhang, 2014), and the resulting cloud geometric thickness information was used to obtain a profile of vertical cloud fraction at FLEXPART-vertical resolutions for each observation point. All vertical cloud fraction profiles (numbering 10,422,219 total profiles over the Arctic Ocean) that fell within 12.5

5   km^2 stereographic projection grid cells (Cavalieri et al., 2014) were then averaged together. The gridded observations over sea ice (open ocean) include 15,999 (31,978) grid cells from fall, 43,687 (24,008) grid cells from winter, and 38,793 (15,289) grid cells from spring, with the observation numbers being a function of sea ice extent and length of darkness periods during each season.

10   Above 1 km, the 2B-GEOPROF-LIDAR product is similar to or better than ground-based observations, but cloud fraction can be underestimated by up to ~20% below ~1 km (Liu et al., 2017), indicating that cloud detection uncertainties in this study's lowest vertical bin (0.6-1.5 km) are higher there than in other altitude ranges.

CloudSat and CALIPSO do not sample north of 82°. The lack of data within this "pole hole" might mean that those sea ice

15   regions are not representatively sampled in this study. It is unclear how well the data outside the pole hole approximate the data inside it, as this region is the coldest part of the Arctic, and probably also contains some of the cleanest parts with respect to aerosols. Also note that thin-ice-cloud identification is particularly prone to errors over the Arctic, due in part to the widespread occurrence of sub-visible diamond dust and blowing snow. Additionally, the CloudSat radar can sometimes mistake precipitation for clouds (de Boer et al., 2009), which can be particularly problematic under optically thick clouds

20   that completely attenuate the CALIPSO lidar signal, and prevent lidar data from being collected below-cloud.

Cloud precipitation presence and phase were obtained from the CloudSat 2B-CLDCLASS-LIDAR version R04 (Wang, 2013). This product captures precipitation with high confidence (Hudak et al., 2008). Phase determination has also been validated favorably at high latitudes (Barker et al., 2008), except that in some cases the radar can misclassify small liquid

25   droplets as ice particles (Noh et al., 2011; Van Tricht et al., 2016). CloudSat may also fail to observe some ice and mixed-phase clouds below 1 km (Liu et al., 2017), suggesting higher uncertainties in cloud phase as well in the lowest vertical bin of this study. Here, cloud phase certainty values were required to be > 5, indicating a higher confidence in phase classification. If a FLEXPART-resolution vertical bin contained clouds of different phases, that bin was excluded from phase-related portions of the analysis. As with CF data, nearby cloud precipitation and phase profile data were averaged

30   within 12.5 km^2 grids at each altitude level prior to analysis.

Estimates of the longwave cloud radiative effect at the bottom-of-the-atmosphere (CRE_{BOA}) were obtained from the CloudSat 2B-FLXHR-LIDAR product, version R04 (Henderson et al., 2012; L'Ecuyer et al., 2008). This product is based on combined CloudSat, CALIPSO, and MODIS observations and time-coincident European Centre for Medium-Range Weather

Forecasts (ECMWF) of atmospheric humidity, temperature and sea surface temperature, fed into the BugsRad two-stream, plane- parallel, doubling-adding radiative transfer model, following Henderson et al. (2012). Previous work shows that this product can severely underestimate downwelling LW radiation due to misclassification of small supercooled water as ice particles (Van Tricht et al., 2016). Therefore, we primarily focus on relative differences in CRE_{BOA} instead of absolute

5   values.

2.3 AIRS observations

Air mass temperature and relative humidity at pressure levels ranging from 1000-250 hPa were obtained from the Atmospheric Infrared Sounder (AIRS) level 3 version 6 dataset (Susskind et al., 2014) on the descending orbit. The AIRS instrument provides quality controlled, accurate daily observations over the full study area, including during nighttime

10   conditions, and is validated for use over the Arctic (Boisvert et al., 2015). Data are available in most cloud conditions, although data are not available in completely cloud-covered conditions. Level 3 data, which average observations over a 1×1° horizontal grid and report at 20 vertical pressure levels, are used instead of level 2 data to obtain closest approximate T and RH data when cloud fractions are high. Errors in this product are highest at larger cloud fractions and below optically thick clouds. For comparison to other datasets in this study, AIRS data were averaged into the coarser FLEXPART model

15   vertical resolution.

2.4 Data analysis

Regionally averaged differences in relative humidity, temperature, and 12.5 km^{2} gridded CF ($\overline{dRH}$, $\overline{dT}$, and $\overline{dCF}$, respectively) between all ($\overline{RH}$, $\overline{T}$, and $\overline{CF}$, respectively) and clean ($\overline{RH_c}$, $\overline{T_c}$, and $\overline{CF_c}$, respectively) conditions were calculated as follows:

(1) $\overline{dRH} = \overline{RH} - \overline{RH_c}$

(2) $\overline{dT} = \overline{T} - \overline{T_c}$

25   (3) $\overline{dCF} = \overline{CF} - \overline{CF_c}$

In a process conceptually fairly similar to previous work (Chen et al., 2014) (see Figure 1 as an example), spatially gridded CF and BC data in all and clean (BC < 30 ng m^{-3}) conditions were sorted into 5% relative humidity bins and 5 ^{o}C temperature bins, and then the differences in all minus clean conditions were compared within each T-RH bin ($dCF_{T,RH}$ and

30   $dBC_{T,RH}$, respectively). We then compared the differences in all minus clean conditions within each T-RH bin for the change in cloud fraction ($dCF_{T,RH}$) black carbon ($dBC_{T,RH}$), cloud phase ($dCP_{T,RH}$) and precipitation frequency ($dpptn_{T,RH}$). Data were analyzed separately over sea ice vs. open ocean, and within different altitude layers.

Stratifying by similar T and RH conditions isolates some of the systematic regional BC co-variability with T and RH, helping clarify the BC aerosol impact on cloud fraction. The 5 $^{\circ}$C T and 5% RH bin increments were chosen to balance the benefits of larger sample sizes against the drawbacks of reduced bin representativeness at smaller bin sizes. Data plotted at
5   larger bin increments resulted in similar trends (data not shown).

The estimated microphysical impact of combustion aerosols on total CF over the Arctic Ocean during polar night is calculated from the mean $dCF_{T,RH}$, weighted by the number of 12.5 km^2 grids containing observations falling within each RH and T bin, abbreviated as $\overline{dCF_{T,RH}}$. Regional averaging helps reduce the effects of horizontal winds on factors such as aerosol
10   advection, which can co-vary on local scales with aerosols (Engström and Ekman, 2010; Nishant and Sherwood, 2017). That, in combination with accounting for variations in the T and RH data, enables us to capture several key meteorological parameters that might influence cloud fraction. However, there are no reliable space-borne measurements for vertical velocity, which might also co-vary systematically with BC on a regional scale, and meteorological reanalyses of large-scale vertical motion over the wintertime Arctic are not well-validated (Jakobson et al., 2012). Our focus on nighttime data over
15   the flat ocean surface likely reduces effects from large-scale vertical motion, but the full uncertainty from this parameter cannot be accounted for here. For example, if cold aerosol-containing continental air is routinely advected over warmer open ocean areas, that could induce systemic convection[36] that might not be fully captured by T and RH. To provide at least some generalized grouping of clouds likely to be influenced by different large-scale vertical motion, we analyzed altitude layers and surface types (sea ice and open ocean) separately.

20   **3 Results**

3.1 Aerosol microphysical effects on cloud fraction

Systematic regional co-variability of aerosols and meteorological factors must be accounted for in order to avoid overestimating aerosol impacts on clouds (Coopman et al., 2018; Gryspeerdt et al., 2016). To illustrate this point, Figure 2 shows the longwave CRE_{BOA} for the upper and lower quartiles of FLEXPART model column BC concentrations during the
25   study period. The upper and lower quartile ranges of column BC levels are associated with very large (~25 W m^{-2}) differences in longwave CRE_{BOA} over sea ice (Fig. 2). However, column BC levels are also associated with noticeable differences in temperature, relative humidity, and lower tropospheric stability (Fig. 2). These meteorological factors strongly affect CF and CP, which in turn help drive CRE_{BOA}. As a result, aerosol microphysical effects may contribute to only a fraction of the CRE_{BOA} differences shown in Figure 2.

30

To help better understand co-varying meteorological effects on CF specifically, we assessed a generalized additive model (GAM) (Hastie and Tibshirani, 1990) of the $\overline{dRH}$, $\overline{dT}$, and $\overline{dCF}$ data at each vertical level, season, and surface type (Table

S1). The GAM suggests that co-varying differences in $\overline{dRH}$ and $\overline{dT}$ by themselves can explain up to 91% of the variability in $\overline{dCF}$ (as measured by deviance, a statistic similar to variance (Jorgensen, 1997)). Because aerosols can co-vary with T and RH (e.g., because polluted air masses are more likely to have recently resided near the continental surface than clean air masses), aerosols could be responsible for some of this explained variability even without being explicitly included in this

5   GAM. Thus, the 91% value is an upper estimate of the $\overline{dRH}$ and $\overline{dT}$ influences. Nonetheless, these findings underscore the importance of interpreting regional-scale aerosol effects on clouds in the context of co-varying temperature and relative humidity. They also indicate that changes in T and RH of air masses entering the Arctic will likely have a very large influence on observed CF, to a degree that is likely to be much more regionally important than the microphysical effects of the aerosols themselves.

Cloud fraction substantially differed among all and clean conditions for many combinations of T, RH, altitude and surface type (Fig. 1). Estimated aerosol impacts on total CF depend on altitude and surface type. At the lowest levels (0.6-2.5 km over sea ice and 0.6-1.5 km over open ocean), weighted mean $dCF_{T,RH}$ ($\overline{dCF_{T,RH}}$) is negative, resulting in an ~6% reduction in CF relative to clean conditions over sea ice (-0.6% over open ocean) (Fig. 3). In contrast, $\overline{dCF_{T,RH}}$ between 4-8.5 km

15   elevation increased by 3-5% over both surfaces, indicating more cloud cover at high altitudes for combustion aerosol influenced clouds compared to clean conditions. Absolute $\overline{dCF_{T,RH}}$ changes over sea ice and open ocean ranged between -1.7% to 0.7% and -0.2 to 1.4%, respectively, depending on altitude.

Although the focus of this work is on regional signals as a whole, it is interesting to note that in Figure 1 over sea ice up to 6

20   km, the $dCF_{T,RH}$ response appears to generally become more positive at constant RH with increasing T (and higher absolute humidity), hinting that combustion aerosols in that environment may be more likely to increase CF when more moisture is available, although a similar effect was not observed over open ocean.

The $dCF_{T,RH}$ and $dBC_{T,RH}$ relationships (Fig. 4) indicate that there was more cloud cover in slightly polluted conditions but

25   less cloud cover at higher $dBC_{T,RH}$ levels (> 10-20 ng m^{-3}) relative to clean conditions. $dCF_{T,RH}$ declined significantly at $dBC_{T,RH}$ > 20 ng m^{-3} within most single altitude layers over sea ice, and over open ocean at 1.5-2.5 km (Table S2).

Note that the fall period typically has cleaner and warmer conditions compared to winter and spring (Table S1), which tend to occur more heavily on opposite sides of the scatter plots for each altitude layer in Figure 4. Thus, any large, systematic

30   differences in the vertical winds between fall and spring could influence the outermost points within individual altitude layers, and it is not easy to control for this effect. However, the trends among altitude layers show that $dCF_{T,RH}$ is essentially identical over sea ice and open ocean at low $dBC_{T,RH}$ values, which occur mostly at high altitudes. Also, $dCF_{T,RH}$ changes at high $dBC_{T,RH}$/low altitude are larger over sea ice (Fig. 4). This finding suggests that aerosol microphysical impacts on clouds

are more influential at the lower temperatures and/or more stable conditions over sea ice. Previous studies have also observed larger aerosol microphysical effects under more stable conditions in the Arctic (Coopman et al., 2018; Zamora et al., 2017). Possible reasons for the disparate behavior at different altitudes are discussed below.

3.2 Aerosol microphysical effects on cloud phase partitioning

5   Weighted mean differences in CP partitioning between all minus clean conditions within the same T and RH bins ($\overline{dCP_{T,RH}}$) are discussed for clouds between 0.6-4 km, because clouds at higher altitudes occur mostly in the ice phase (Fig. 3) (Devasthale et al., 2011a; Liu et al., 2017). Over sea ice between 0.6-4 km, all air masses contained a higher relative fraction of ice phase clouds (IPCs) and a lower relative fraction of liquid phase clouds (LPCs) and mixed phase clouds (MPCs) relative to all air masses (Fig. 3). This effect was significant up to 4 km (paired Wilcoxon rank test (Sokal and Rohlf, 1995),

10   $p < 0.05$), except in LPCs between 2.5-4 km, where lower sample numbers might obscure any changes. Regional-scale changes in phase partitioning varied between -4.2 and 6.5%, depending on altitude and phase (Fig. 3). Over sea ice between 1.5-2.5 km, the relative contributions of LPCs and MPCs were significantly lower at high $dBC_{T,RH}$ levels (>20 ng m^{-3}), whereas that of IPCs was significantly higher (Table S2). No significant relationships with $dBC_{T,RH}$ were observed above or below that altitude, although higher BC and CP uncertainties near the surface might mask weak signals in that altitude range.

Over open ocean, significant changes in $\overline{dCP_{T,RH}}$ were observed less frequently (Fig. 3), and they tended to be smaller than over sea ice (absolute values < 2%). The relative fraction of liquid clouds was reduced between 0.6-1.5 km, where LPC fractions were highest (Fig. 3). However, unlike over sea ice, the relative fraction of MPCs over open ocean increased (though not significantly so between 1.5-2.5 km), and that of IPCs decreased (significant only between 2.5-4 km).

3.3 Aerosol microphysical influences on precipitation frequency

Differences in precipitation frequency, $dpptn_{T,RH}$, reflect aerosol microphysical impacts on: 1) the frequency of precipitation within a specific air volume, and 2) the relative likelihood of individual cloud phases within that air volume to be precipitating. An analysis of total precipitation amounts or precipitating particle microphysics is beyond the scope of this study.

25

Based on weighted mean $dpptn_{T,RH}$ values ($\overline{dpptn_{T,RH}}$), estimated aerosol microphysical effects on regional precipitation frequency were small but significant at many altitudes (Fig. 3, Fig. S2). In all air mass conditions, precipitation frequency was 1.2-3.1% higher below 6 km over open ocean and below 1.5 km over sea ice relative to clean conditions, depending on altitude (Fig. 3). In contrast, clean clouds between 6-8.5 km over open ocean were slightly more likely to be precipitating

30   ($\overline{dpptn_{T,RH}}$ ~ -1%).

Over sea ice, ~91% of MPCs were present below 4 km. In these MPCs, $\overline{dpptn_{T,RH}}$ was positive (~ +1%), indicating slightly more frequent precipitation on average in all vs. clean MPCs (Fig. 3b). Significant differences between all and clean conditions were not observed for $\overline{dpptn_{T,RH}}$ in IPCs or LPCs over sea ice, except for a slight (-0.4%) reduction in $\overline{dpptn_{T,RH}}$ in ice clouds at 6-8.5 km (Fig. 3b). However, significant rank correlations (Kendall's tau coefficient = 0.3, p < 0.05) indicate

5   that higher $dBC_{T,RH}$ values were associated with slightly more frequent IPC precipitation over sea ice between 0.6-1.5 km (also see Fig. S1). We observed no strong link between $dBC_{T,RH}$ and $dpptn_{T,RH}$ at other locations/altitudes.

As over sea ice, MPC $\overline{dpptn_{T,RH}}$ was slightly positive (≤1%) below 4 km over open ocean (Fig. 3b), indicating slightly more MPC precipitation in all vs. clean conditions. IPC $\overline{dpptn_{T,RH}}$ was also slightly positive between 1.5-4 km, whereas liquid

10   cloud $\overline{dpptn_{T,RH}}$ was slightly negative between 1.5-4 km. Between 6-8.5 km over open ocean, the $\overline{dpptn_{T,RH}}$ in MPCs was slightly negative at ~-1% (Fig. 3).

Based on single or small cloud samples, others have observed decreased precipitation probability with increased aerosol concentrations in Arctic MPCs (Lance et al., 2011; Morrison et al., 2008). It is not entirely clear why the regional trends

15   observed here appear to be opposite these smaller-scale *in situ* observations, but recent work indicates that aerosols might influence ice content of the clouds, and thereby affect precipitation (Fu and Xue, 2017; Norgren et al., 2018; Zamora et al., 2017) and potentially CF. Perhaps lower total CF below 4 km leads to less frequent precipitation in these air volumes over the Arctic. The higher MPC precipitation probability and lower MPC cover (as indicated by reduced MPC relative fraction of total CF) at higher aerosol concentrations support this hypothesis.

20   **4 Discussion – Potential aerosol microphysical mechanisms**

Specific aerosol-cloud microphysical mechanisms are difficult to identify with confidence from space-borne measurements alone, but some possibilities can be explored. At high altitudes (6-8.5 km) over sea ice, $\overline{dCF_{T,RH}}$ was higher and $\overline{dpptn_{T,RH}}$ was lower in all vs. clean conditions (Fig. 3), supporting the hypothesis that aerosols are modifying cloud properties on a regional scale at these altitudes, even though the net changes were relatively small. These modifications to predominantly

25   IPCs at high altitude likely involve aerosol effects on ice crystal formation or properties. Oreopoulos et al.(2017) similarly reported global-scale increases in ice CF with higher aerosol concentration in their CR1 cases (typically high ice clouds of small optical thickness over the tropics), which was linked to reduced ice cloud effective radius.

There are several mechanisms by which aerosol might modify ice crystal number or size that could cause the observed

30   changes in precipitation and CF in the 6-8.5 km range. Combustion aerosols associated with BC might act as ice nucleating particles (INPs) (Kanji et al., 2017) at the extreme cold temperatures found at high-altitude Arctic polar night, potentially leading to smaller, more numerous ice particles that precipitate less (Lohmann and Feichter, 2005), although some models

suggest that INPs may instead lead to larger ice crystals in cirrus clouds compared to homogeneous freezing (Heymsfield et al., 2016). Alternatively, combustion aerosols might reduce the efficiency of pre-existing INPs through the "deactivation effect" (Archuleta et al., 2005; Cziczo et al., 2009). Reduced ice crystal formation rates could then lead to more frequent air mass saturation with respect to liquid water, more water droplets that freeze homogeneously, and smaller, more numerous

5   ice particles, and less precipitation (Girard et al., 2013). This effect could lead to enhanced total CF over the Arctic (Du et al., 2011). Although absolute humidity within the different T-RH bins between 6-8.5 km is not systematically related to higher $dBC_{T,RH}$ levels as one might expect with the deactivation effect, it is possible that pre-sorting the data by 5% RH bins to reduce the impacts of meteorological co-variation could make evidence for this effect more difficult to observe.

10 The specific microphysical mechanisms affecting lower altitude clouds are more challenging to identify without in situ data due to the high prevalence of liquid-containing clouds (Fig. 3). Once T and RH co-variability are accounted for, all air masses at low altitudes (0.6 to 1.5-2.5 km) have lower CF compared to clean conditions. They also have more frequent precipitation in IPCs at high $dBC_{T,RH}$, and a higher relative fraction of IPCs over sea ice and MPCs over the warmer open ocean. Each of these changes is significantly different between low and high $dBC_{T,RH}$ concentrations at a variety of altitudes

15 and surface types (Table S2), suggesting that aerosols may help convert liquid droplets to larger ice particles that precipitate out and reduce CF in lower altitude clouds (e.g., via the glaciation effect (Lohmann, 2002)).

These observations are in-line with other studies indicating that aerosols can dissipate Arctic MPCs (Fu and Xue, 2017; Norgren et al., 2018), and a remote sensing study indicating an association between smoke aerosols and reduced supercooled

20 water frequency (Tan et al., 2014). The observations over sea ice contrast with some model predictions that MPCs should increase in more polluted conditions through the deactivation effect (Du et al., 2011; Girard et al., 2005, 2013). They also contrast with a previous remote sensing study (Zamora et al., 2017) indicating that thin and predominantly liquid Arctic Ocean clouds are more likely to be the liquid phase at high BC concentrations. However, the clouds in that study may not be fully comparable, as they constitute only ~5% of the cloud types in this study. Note that shortwave processes might alter how

25 aerosols impact mixed phase CF during daytime (Solomon et al., 2015), and any such effects would not be observed in the current, nighttime study. Changes in higher altitude clouds might also change underlying cloud properties through a seeding effect, which could impact cloud properties at lower altitudes.

5 Summary and conclusions

Upper quartile levels of total column BC (a proxy for combustion aerosols) are associated with very large (~25 W m^{-2})

30 differences in longwave cloud radiative effects at the sea ice surface compared to the lower quartile column BC levels. However, relative humidity in particular over sea ice is very different in the two aerosol conditions, which likely drives much of the CRE_{BOA} differences in Figure 2. The CRE_{BOA} is impacted to a high degree by CF. We found that AIRS-derived

temperature and relative humidity predicted up to 91% of the observed regional-scale differences in CF between all and clean conditions in the altitude ranges of interest in this study (0.6-8.5 km). These observations indicate that changes in T and RH of air masses entering the Arctic will likely have a very large influence on observed CF, to a degree that is much more regionally important than the microphysical effects of the aerosols themselves. In line with previous studies (e.g.,
5 Gryspeerdt et al. (2016); Coopman et al. (2018)), these results also underscore the need for large sample volumes to identify systematic differences in regional air masses between clean and all conditions, and a way to reduce the confounding effects of meteorological co-variation on these samples. To accomplish this, we analyzed over 10 million profiles across the Arctic Ocean, which were binned into similar T and RH groups. We analyzed the data separately over sea ice vs. open ocean, and within different altitude layers.

In general, aerosol microphysical effects were most observable where the highest aerosol effect would be expected: at lower altitudes where aerosol concentrations are often higher (Devasthale et al., 2011b) and over sea ice, where atmospheric stability is greater. Relative to clean conditions, low clouds over sea ice had ~6% smaller CF and 3% higher precipitation frequency, whereas at high altitudes, CF increased by 4% and precipitation was 2% less frequent. Similar but smaller trends
15 in CF and low-altitude precipitation were observed over open ocean. Below 1.5 km, we also observed a 7% reduction in the LPC and MPC fractions over sea ice, but a slight increase in MPCs relative to IPCs and LPCs over open ocean.

These results are subject to various uncertainties, including possible confounding influences from large-scale vertical motion that is difficult to measure in situ, any systematic model errors in identifying aerosol layers at the right altitude (see
20 supplementary information), and the uncertain relationships between modeled BC and INP and cloud condensation nuclei (CCN) concentrations. Associations between $dBC_{T,RH}$ and cloud properties may be difficult to observe given the low BC concentrations at altitudes > 4 km, and may be further masked by complex aerosol-cloud relationships. Despite these uncertainties, significant differences in $dCF_{T,RH}$, $dpptn_{T,RH}$, and $dCP_{T,RH}$ at high $dBC_{T,RH}$ concentrations provide evidence that aerosol microphysical effects were driving the observed patterns, as opposed to some other factor. Furthermore, these
25 observations leave open the possibility that other cloud property relationships with $dBC_{T,RH}$ exist, but are not observable with the available data.

The mechanisms responsible for these changes cannot be fully elucidated from modeling and remote sensing data alone. The observed increases in CF and decreases in precipitation at 6-8.5 km likely involve aerosol effects on ice crystal formation or
30 properties, given that nearly all of these clouds are in the ice phase. These effects might include a deactivation of pre-existing INPs, or conversely an enhancement of INPs by combustion aerosols themselves at the very low temperatures observed at these high altitudes during Arctic polar night. The reduced CF, more frequent precipitation in mixed phase clouds, and reduced relative fraction of mixed (liquid) phase clouds over sea ice (open ocean) seem to point towards aerosols either

participating in the conversion of liquid droplets to larger ice particles that precipitate and reduce CF, similar to a glaciation effect, or potentially to their impacts on precipitation in higher clouds, changing underlying cloud properties through a seeding effect. Further focused studies on these mechanisms would be of great interest, along with targeted aircraft measurements of the relevant aerosol and cloud properties, providing greater detail at higher spatial and temporal resolution.

5 To improve quantification of Arctic aerosol-cloud microphysical interactions from space, two major uncertainties also require better quantification: (1) large-scale vertical motion and (2) altitude-resolved aerosol amount and type information. Obtaining more ground-based observations of clouds lower than 0.6 km, which are radiatively significant but not measured well by satellite, is also important.

10 **Acknowledgements**

The authors would like to thank A. Ackerman, G. De Boer, J. Creamean, A. Fridlind, B. Hegyi, K.-M. Kim, J. Limbacher, G. McFarquhar, L. Oreopoulos, and J. Susskind for helpful discussions. CALIPSO data were provided by the NASA Langley Research Center Atmospheric Science Data Center, and the CIRA CloudSat Data Processing Center provided the CloudSat data. The work of L.M.Z. and R.A.K. is supported in part by NASA's Climate and Radiation Research and Analysis
15 Program under H. Maring and NASA's Atmospheric Composition Program under R. Eckman and K. Jucks.

References

Albrecht, B. A.: Aerosols, Cloud Microphysics, and Fractional Cloudiness, Science, 245(4923), 1227–1230, doi:10.1126/science.245.4923.1227, 1989.

Amante, C. and Eakins, B. W.: ETOPO1 1 Arc-Minute Global Relief Model: Procedures, Data Sources and Analysis.
20 NOAA Technical Memorandum NESDIS NGDC-24. National Geophysical Data Center, NOAA., , doi:10.7289/V5C8276M, 2009.

Archuleta, C. M., DeMott, P. J. and Kreidenweis, S. M.: Ice nucleation by surrogates for atmospheric mineral dust and mineral dust/sulfate particles at cirrus temperatures, Atmos Chem Phys, 5(10), 2617–2634, doi:10.5194/acp-5-2617-2005, 2005.

25 Barker, H. W., Korolev, A. V., Hudak, D. R., Strapp, J. W., Strawbridge, K. B. and Wolde, M.: A comparison between CloudSat and aircraft data for a multilayer, mixed phase cloud system during the Canadian CloudSat-CALIPSO Validation Project, J. Geophys. Res. Atmospheres, 113(D8), D00A16, doi:10.1029/2008JD009971, 2008.

de Boer, G., Eloranta, E. W. and Shupe, M. D.: Arctic Mixed-Phase Stratiform Cloud Properties from Multiple Years of Surface-Based Measurements at Two High-Latitude Locations, J. Atmospheric Sci., 66(9), 2874–2887,
30 doi:10.1175/2009JAS3029.1, 2009.

de Boer, G., Chapman, W., Kay, J. E., Medeiros, B., Shupe, M. D., Vavrus, S. and Walsh, J.: A Characterization of the Present-Day Arctic Atmosphere in CCSM4, J. Clim., 25(8), 2676–2695, doi:10.1175/JCLI-D-11-00228.1, 2011.

Boisvert, L. N. and Stroeve, J. C.: The Arctic is becoming warmer and wetter as revealed by the Atmospheric Infrared Sounder, Geophys. Res. Lett., 42(11), 4439–4446, doi:10.1002/2015GL063775, 2015.

Boisvert, L. N., Wu, D. L., Vihma, T. and Susskind, J.: Verification of air/surface humidity differences from AIRS and ERA-Interim in support of turbulent flux estimation in the Arctic, J. Geophys. Res. Atmospheres, 120(3), 2014JD021666, doi:10.1002/2014JD021666, 2015.

Boucher, O., Randall, D. A., Artaxo, P., Bretherton, C. S., Feingold, G., Forster, P. M., Kerminen, V.-M., Kondo, Y., Liao, H., Lohmann, U., Rasch, P., Satheesh, S. K., Sherwood, S., Stevens, B. and Zhang, X. Y.: Clouds and Aerosols, in Climate Change 2013: The Physical Science Basis. Contribution of Working Group I to the Fifth Assessment Report of the Intergovernmental Panel on Climate Change, edited by T. F. Stocker, D. Qin, G. K. Plattner, M. Tignor, S. K. Allen, J. Boschung, A. Nauels, Y. Xia, V. Bex, and P. M. Midgley, Cambridge University Press, Cambridge, UK and New York, NY, USA., 2013.

Cavalieri, D. J., Markus, T. and Comiso, J.: AMSR-E/Aqua Daily L3 12.5 km Brightness Temperature, Sea Ice Concentration, & Snow Depth Polar Grids, Version 3, psn12area_v3.dat. Boulder, Colorado USA. NASA National Snow and Ice Data Center Distributed Active Archive Center. doi: http://dx.doi.org/10.5067/AMSR-E/AE_SI12.003. Accessed Aug. 11, 2017, 2014.

Cesana, G. and Chepfer, H.: How well do climate models simulate cloud vertical structure? A comparison between CALIPSO-GOCCP satellite observations and CMIP5 models, Geophys. Res. Lett., 39(20), L20803, doi:10.1029/2012GL053153, 2012.

Chen, Y.-C., Christensen, M. W., Stephens, G. L. and Seinfeld, J. H.: Satellite-based estimate of global aerosol-cloud radiative forcing by marine warm clouds, Nat. Geosci., 7(9), 643–646, doi:10.1038/ngeo2214, 2014.

Chernokulsky, A. and Mokhov, I. I.: Climatology of Total Cloudiness in the Arctic: An Intercomparison of Observations and Reanalyses, Adv. Meteorol., doi:10.1155/2012/542093, 2012.

Coopman, Q., Garrett, T. J., Riedi, J., Eckhardt, S. and Stohl, A.: Effects of long-range aerosol transport on the microphysical properties of low-level liquid clouds in the Arctic, Atmos Chem Phys, 16(7), 4661–4674, doi:10.5194/acp-16-4661-2016, 2016.

Coopman, Q., Garrett, T. J., Finch, D. P. and Riedi, J.: High Sensitivity of Arctic Liquid Clouds to Long-Range Anthropogenic Aerosol Transport, Geophys. Res. Lett., 45(1), 372–381, doi:10.1002/2017GL075795, 2018.

Creamean, J. M., Maahn, M., de Boer, G., McComiskey, A., Sedlacek, A. J. and Feng, Y.: The influence of local oil exploration and regional wildfires on summer 2015 aerosol over the North Slope of Alaska, Atmos Chem Phys, 18(2), 555–570, doi:10.5194/acp-18-555-2018, 2018.

Cziczo, D. J., Froyd, K. D., Gallavardin, S. J., Moehler, O., Benz, S., Harald Saathoff and Murphy, D. M.: Deactivation of ice nuclei due to atmospherically relevant surface coatings, Environ. Res. Lett., 4(4), 044013, doi:10.1088/1748-9326/4/4/044013, 2009.

Damoah, R., Spichtinger, N., Forster, C., James, P., Mattis, I., Wandinger, U., Beirle, S., Wagner, T. and Stohl, A.: Around the world in 17 days - hemispheric-scale transport of forest fire smoke from Russia in May 2003, Atmos Chem Phys, 4(5), 1311–1321, doi:10.5194/acp-4-1311-2004, 2004.

Devasthale, A., TjernströM, M., Karlsson, K.-G., Thomas, M. A., Jones, C., Sedlar, J. and Omar, A. H.: The vertical distribution of thin features over the Arctic analysed from CALIPSO observations, Part I: Optically thin clouds, Tellus B, 63(1), 77–85, doi:10.1111/j.1600-0889.2010.00516.x, 2011a.

Devasthale, A., Tjernström, M. and Omar, A. H.: The vertical distribution of thin features over the Arctic analysed from CALIPSO observations. Part II: Aerosols, Tellus B, 63(1), doi:10.3402/tellusb.v63i1.16190, 2011b.

Du, P., Girard, E., Bertram, A. K. and Shupe, M. D.: Modeling of the cloud and radiation processes observed during SHEBA, Atmospheric Res., 101(4), 911–927, doi:10.1016/j.atmosres.2011.05.018, 2011.

Eckhardt, S., Quennehen, B., Olivié, D. J. L., Berntsen, T. K., Cherian, R., Christensen, J. H., Collins, W., Crepinsek, S., Daskalakis, N., Flanner, M., Herber, A., Heyes, C., Hodnebrog, Ø., Huang, L., Kanakidou, M., Klimont, Z., Langner, J., Law, K. S., Lund, M. T., Mahmood, R., Massling, A., Myriokefalitakis, S., Nielsen, I. E., Nøjgaard, J. K., Quaas, J., Quinn, P. K., Raut, J.-C., Rumbold, S. T., Schulz, M., Sharma, S., Skeie, R. B., Skov, H., Uttal, T., von Salzen, K. and Stohl, A.: Current model capabilities for simulating black carbon and sulfate concentrations in the Arctic atmosphere: a multi-model evaluation using a comprehensive measurement data set, Atmos Chem Phys, 15(16), 9413–9433, doi:10.5194/acp-15-9413-2015, 2015.

Engström, A. and Ekman, A. M. L.: Impact of meteorological factors on the correlation between aerosol optical depth and cloud fraction, Geophys. Res. Lett., 37(18), doi:10.1029/2010GL044361, 2010.

Fan, J., Wang, Y., Rosenfeld, D. and Liu, X.: Review of Aerosol–Cloud Interactions: Mechanisms, Significance, and Challenges, J. Atmospheric Sci., 73(11), 4221–4252, doi:10.1175/JAS-D-16-0037.1, 2016.

Forster, C., Wandinger, U., Wotawa, G., James, P., Mattis, I., Althausen, D., Simmonds, P., O'Doherty, S., Jennings, S. G., Kleefeld, C., Schneider, J., Trickl, T., Kreipl, S., Jäger, H. and Stohl, A.: Transport of boreal forest fire emissions from Canada to Europe, J. Geophys. Res. Atmospheres, 106(D19), 22887–22906, doi:10.1029/2001JD900115, 2001.

Fu, S. and Xue, H.: The Effect of Ice Nuclei Efficiency on Arctic Mixed-Phase Clouds from Large-Eddy Simulations, J. Atmospheric Sci., 74(12), 3901–3913, doi:10.1175/JAS-D-17-0112.1, 2017.

Giglio, L., Randerson, J. T. and Werf, G. R.: Analysis of daily, monthly, and annual burned area using the fourth-generation global fire emissions database (GFED4), J. Geophys. Res. Biogeosciences, 118(1), 317–328, doi:10.1002/jgrg.20042, 2013.

Girard, E., Blanchet, J.-P. and Dubois, Y.: Effects of arctic sulphuric acid aerosols on wintertime low-level atmospheric ice crystals, humidity and temperature at Alert, Nunavut, Atmospheric Res., 73(1–2), 131–148, doi:10.1016/j.atmosres.2004.08.002, 2005.

Girard, E., Dueymes, G., Du, P. and Bertram, A. K.: Assessment of the effects of acid-coated ice nuclei on the Arctic cloud microstructure, atmospheric dehydration, radiation and temperature during winter, Int. J. Climatol., 33(3), 599–614, doi:10.1002/joc.3454, 2013.

Gryspeerdt, E., Quaas, J. and Bellouin, N.: Constraining the aerosol influence on cloud fraction, J. Geophys. Res. Atmospheres, 121(7), 3566–3583, doi:10.1002/2015JD023744, 2016.

Hastie, T. J. and Tibshirani, R. J.: Generalized Additive Models, Chapman and Hall, London., 1990.

Henderson, D. S., L'Ecuyer, T., Stephens, G., Partain, P. and Sekiguchi, M.: A Multisensor Perspective on the Radiative Impacts of Clouds and Aerosols, J. Appl. Meteorol. Climatol., 52(4), 853–871, doi:10.1175/JAMC-D-12-025.1, 2012.

Heymsfield, A. J., Krämer, M., Luebke, A., Brown, P., Cziczo, D. J., Franklin, C., Lawson, P., Lohmann, U., McFarquhar, G., Ulanowski, Z. and Van Tricht, K.: Cirrus Clouds, Meteorol. Monogr., 58, 2.1-2.26, doi:10.1175/AMSMONOGRAPHS-D-16-0010.1, 2016.

Hudak, D., Rodriguez, P. and Donaldson, N.: Validation of the CloudSat precipitation occurrence algorithm using the Canadian C band radar network, J. Geophys. Res. Atmosheres, 113(D8), D00A07, doi:10.1029/2008JD009992, 2008.

Jakobson, E., Vihma, T., Palo, T., Jakobson, L., Keernik, H. and Jaagus, J.: Validation of atmospheric reanalyses over the central Arctic Ocean, Geophys. Res. Lett., 39(10), L10802, doi:10.1029/2012GL051591, 2012.

Jorgensen, B.: The Theory of Dispersion, Chapman and Hall., 1997.

Kanji, Z. A., Ladino, L. A., Wex, H., Boose, Y., Burkert-Kohn, M., Cziczo, D. J. and Krämer, M.: Overview of Ice Nucleating Particles, Meteorol. Monogr., 58, 1.1-1.33, doi:10.1175/AMSMONOGRAPHS-D-16-0006.1, 2017.

Kay, J. E. and L'Ecuyer, T.: Observational constraints on Arctic Ocean clouds and radiative fluxes during the early 21st century, J. Geophys. Res. Atmosheres, 118(13), 7219–7236, doi:10.1002/jgrd.50489, 2013.

Kay, J. E., Raeder, K., Gettelman, A. and Anderson, J.: The Boundary Layer Response to Recent Arctic Sea Ice Loss and Implications for High-Latitude Climate Feedbacks, J. Clim., 24(2), 428–447, doi:10.1175/2010JCLI3651.1, 2010.

Lance, S., Shupe, M. D., Feingold, G., Brock, C. A., Cozic, J., Holloway, J. S., Moore, R. H., Nenes, A., Schwarz, J. P., Spackman, J. R., Froyd, K. D., Murphy, D. M., Brioude, J., Cooper, O. R., Stohl, A. and Burkhart, J. F.: Cloud condensation nuclei as a modulator of ice processes in Arctic mixed-phase clouds, Atmospheric Chem. Phys., 11(15), 8003–8015, 2011.

L'Ecuyer, T. S., Wood, N. B., Haladay, T., Stephens, G. L. and Stackhouse, P. W.: Impact of clouds on atmospheric heating based on the R04 CloudSat fluxes and heating rates data set, J. Geophys. Res. Atmosheres, 113(D8), D00A15, doi:10.1029/2008JD009951, 2008.

Lindsey, D. T. and Fromm, M.: Evidence of the cloud lifetime effect from wildfire-induced thunderstorms, Geophys. Res. Lett., 35(22), L22809, doi:10.1029/2008GL035680, 2008.

Liu, X., Xie, S., Boyle, J., Klein, S. A., Shi, X., Wang, Z., Lin, W., Ghan, S. J., Earle, M., Liu, P. S. K. and Zelenyuk, A.: Testing cloud microphysics parameterizations in NCAR CAM5 with ISDAC and M-PACE observations, J. Geophys. Res. Atmosheres, 116(D1), D00T11, doi:10.1029/2011JD015889, 2011.

Liu, Y., Shupe, M. D., Wang, Z. and Mace, G.: Cloud vertical distribution from combined surface and space radar–lidar observations at two Arctic atmospheric observatories, Atmos Chem Phys, 17(9), 5973–5989, doi:10.5194/acp-17-5973-2017, 2017.

Lohmann, U.: A glaciation indirect aerosol effect caused by soot aerosols, Geophys. Res. Lett., 29(4), 11–1, doi:10.1029/2001GL014357, 2002.

Lohmann, U. and Feichter, J.: Global indirect aerosol effects: a review, Atmos Chem Phys, 5(3), 715–737, doi:10.5194/acp-5-715-2005, 2005.

Maahn, M., de Boer, G., Creamean, J. M., Feingold, G., McFarquhar, G. M., Wu, W. and Mei, F.: The observed influence of local anthropogenic pollution on northern Alaskan cloud properties, Atmos Chem Phys, 17(23), 14709–14726, doi:10.5194/acp-17-14709-2017, 2017.

Mace, G. G. and Zhang, Q.: The CloudSat radar-lidar geometrical profile product (RL-GeoProf): Updates, improvements, and selected results, J. Geophys. Res. Atmospheres, 119(15), 2013JD021374, doi:10.1002/2013JD021374, 2014.

Mace, G. G., Zhang, Q., Vaughan, M., Marchand, R., Stephens, G., Trepte, C. and Winker, D.: A description of hydrometeor layer occurrence statistics derived from the first year of merged Cloudsat and CALIPSO data, J. Geophys. Res. Atmospheres, 114(D8), D00A26, doi:10.1029/2007JD009755, 2009.

Meier, W., Fetterer, F., Savoie, M., Mallory, S., Duerr, R. and Stroeve, J. C.: NOAA/NSIDC Climate Data Record of Passive Microwave Sea Ice Concentration, Version 2. [G02202], NSIDC: National Snow and Ice Data Center, Boulder, Colorado, USA. [online] Available from: doi: http://dx.doi.org/10.7265/N55M63M1 (Accessed 23 May 2016), 2013.

Morrison, H., Pinto, J. O., Curry, J. A. and McFarquhar, G. M.: Sensitivity of modeled arctic mixed-phase stratocumulus to cloud condensation and ice nuclei over regionally varying surface conditions, J. Geophys. Res. Atmospheres, 113(D5), D05203, doi:10.1029/2007JD008729, 2008.

Morrison, H., de Boer, G., Feingold, G., Harrington, J., Shupe, M. D. and Sulia, K.: Resilience of persistent Arctic mixed-phase clouds, Nat. Geosci., 5(1), 11–17, doi:10.1038/ngeo1332, 2012.

Nishant, N. and Sherwood, S. C.: A cloud-resolving model study of aerosol-cloud correlation in a pristine maritime environment, Geophys. Res. Lett., 44(11), 5774–5781, doi:10.1002/2017GL073267, 2017.

Noh, Y.-J., Seaman, C. J., Vonder Haar, T. H., Hudak, D. R. and Rodriguez, P.: Comparisons and analyses of aircraft and satellite observations for wintertime mixed-phase clouds, J. Geophys. Res. Atmospheres, 116(D18), D18207, doi:10.1029/2010JD015420, 2011.

Norgren, M. S., de Boer, G. and Shupe, M. D.: Observed aerosol suppression of cloud ice in low-level Arctic mixed-phase clouds, Atmos Chem Phys Discuss, 2018, 1–25, doi:10.5194/acp-2017-1191, 2018.

Oreopoulos, L., Cho, N. and Lee, D.: Using MODIS cloud regimes to sort diagnostic signals of aerosol-cloud-precipitation interactions, J. Geophys. Res. Atmospheres, 122(10), 5416–5440, doi:10.1002/2016JD026120, 2017.

Paris, J.-D., Stohl, A., Nédélec, P., Arshinov, M. Y., Panchenko, M. V., Shmargunov, V. P., Law, K. S., Belan, B. D. and Ciais, P.: Wildfire smoke in the Siberian Arctic in summer: source characterization and plume evolution from airborne measurements, Atmos Chem Phys, 9(23), 9315–9327, doi:10.5194/acp-9-9315-2009, 2009.

Peng, G., Meier, W. N., Scott, D. J. and Savoie, M. H.: A long-term and reproducible passive microwave sea ice concentration data record for climate studies and monitoring, Earth Syst. Sci. Data, 5(2), 311–318, doi:10.5194/essd-5-311-2013, 2013.

Qian, Y., Long, C. N., Wang, H., Comstock, J. M., McFarlane, S. A. and Xie, S.: Evaluation of cloud fraction and its radiative effect simulated by IPCC AR4 global models against ARM surface observations, Atmos Chem Phys, 12(4), 1785–1810, doi:10.5194/acp-12-1785-2012, 2012.

Russell, P. B., Kacenelenbogen, M., Livingston, J. M., Hasekamp, O. P., Burton, S. P., Schuster, G. L., Johnson, M. S., Knobelspiesse, K. D., Redemann, J., Ramachandran, S. and Holben, B.: A multiparameter aerosol classification method and its application to retrievals from spaceborne polarimetry, J. Geophys. Res. Atmospheres, 119(16), 2013JD021411, doi:10.1002/2013JD021411, 2014.

Samset, B. H., Stjern, C. W., Andrews, E., Kahn, R. A., Myhre, G., Schulz, M. and Schuster, G. L.: Aerosol Absorption: Progress Towards Global and Regional Constraints, Curr. Clim. Change Rep., 1–19, doi:10.1007/s40641-018-0091-4, 2018.

Serreze, M. C. and Barry, R. G.: The Arctic Climate System, Camb. Core, doi:10.1017/CBO9780511535888, 2005.

Sodemann, H., Pommier, M., Arnold, S. R., Monks, S. A., Stebel, K., Burkhart, J. F., Hair, J. W., Diskin, G. S., Clerbaux, C., Coheur, P.-F., Hurtmans, D., Schlager, H., Blechschmidt, A.-M., Kristjánsson, J. E. and Stohl, A.: Episodes of cross-polar transport in the Arctic troposphere during July 2008 as seen from models, satellite, and aircraft observations, Atmos Chem Phys, 11(8), 3631–3651, doi:10.5194/acp-11-3631-2011, 2011.

Södergren, A. H., McDonald, A. J. and Bodeker, G. E.: An energy balance model exploration of the impacts of interactions between surface albedo, cloud cover and water vapor on polar amplification, Clim. Dyn., 1–20, doi:10.1007/s00382-017-3974-5, 2017.

Sokal, R. R. and Rohlf, F. J.: Biometry: The Principles and Practice of Statistics in Biological Research, 3rd ed., Macmillan., 1995.

Solomon, A., Feingold, G. and Shupe, M. D.: The role of ice nuclei recycling in the maintenance of cloud ice in Arctic mixed-phase stratocumulus, Atmos Chem Phys, 15(18), 10631–10643, doi:10.5194/acp-15-10631-2015, 2015.

Stanfield, R. E., Dong, X., Xi, B., Kennedy, A., Del Genio, A. D., Minnis, P. and Jiang, J. H.: Assessment of NASA GISS CMIP5 and Post-CMIP5 Simulated Clouds and TOA Radiation Budgets Using Satellite Observations. Part I: Cloud Fraction and Properties, J. Clim., 27(11), 4189–4208, doi:10.1175/JCLI-D-13-00558.1, 2014.

Stevens, R. G., Loewe, K., Dearden, C., Dimitrelos, A., Possner, A., Eirund, G. K., Raatikainen, T., Hill, A. A., Shipway, B. J., Wilkinson, J., Romakkaniemi, S., Tonttila, J., Laaksonen, A., Korhonen, H., Connolly, P., Lohmann, U., Hoose, C., Ekman, A. M. L., Carslaw, K. S. and Field, P. R.: A Model Intercomparison of CCN-Limited Tenuous Clouds in the High Arctic, Atmos Chem Phys Discuss, 2017, 1–42, doi:10.5194/acp-2017-1128, 2017.

Stohl, A., Hittenberger, M. and Wotawa, G.: Validation of the lagrangian particle dispersion model FLEXPART against large-scale tracer experiment data, Atmos. Environ., 32(24), 4245–4264, doi:10.1016/S1352-2310(98)00184-8, 1998.

Stohl, A., Eckhardt, S., Forster, C., James, P. and Spichtinger, N.: On the pathways and timescales of intercontinental air pollution transport, J. Geophys. Res. Atmospheres, 107(D23), 4684, doi:10.1029/2001JD001396, 2002.

Stohl, A., Forster, C., Eckhardt, S., Spichtinger, N., Huntrieser, H., Heland, J., Schlager, H., Wilhelm, S., Arnold, F. and Cooper, O.: A backward modeling study of intercontinental pollution transport using aircraft measurements, J. Geophys. Res. Atmospheres, 108(D12), 4370, doi:10.1029/2002JD002862, 2003.

Stohl, A., Forster, C., Frank, A., Seibert, P. and Wotawa, G.: Technical note: The Lagrangian particle dispersion model FLEXPART version 6.2, Atmos Chem Phys, 5(9), 2461–2474, doi:10.5194/acp-5-2461-2005, 2005.

Stohl, A., Aamaas, B., Amann, M., Baker, L. H., Bellouin, N., Berntsen, T. K., Boucher, O., Cherian, R., Collins, W., Daskalakis, N., Dusinska, M., Eckhardt, S., Fuglestvedt, J. S., Harju, M., Heyes, C., Hodnebrog, Ø., Hao, J., Im, U., Kanakidou, M., Klimont, Z., Kupiainen, K., Law, K. S., Lund, M. T., Maas, R., MacIntosh, C. R., Myhre, G., Myriokefalitakis, S., Olivié, D., Quaas, J., Quennehen, B., Raut, J.-C., Rumbold, S. T., Samset, B. H., Schulz, M., Seland, Ø., Shine, K. P., Skeie, R. B., Wang, S., Yttri, K. E. and Zhu, T.: Evaluating the climate and air quality impacts of short-lived pollutants, Atmos Chem Phys, 15(18), 10529–10566, doi:10.5194/acp-15-10529-2015, 2015.

Susskind, J., Blaisdell, J. M. and Iredell, L.: Improved methodology for surface and atmospheric soundings, error estimates, and quality control procedures: the atmospheric infrared sounder science team version-6 retrieval algorithm, J. Appl. Remote Sens., 8(1), 084994, doi:10.1117/1.JRS.8.084994, 2014.

Tan, I., Storelvmo, T. and Choi, Y.-S.: Spaceborne lidar observations of the ice-nucleating potential of dust, polluted dust,

5 and smoke aerosols in mixed-phase clouds, J. Geophys. Res. Atmospheres, 119(11), 6653–6665, doi:10.1002/2013JD021333, 2014.

Van Tricht, K., Lhermitte, S., Lenaerts, J. T. M., Gorodetskaya, I. V., L'Ecuyer, T. S., Noël, B., van den Broeke, M. R., Turner, D. D. and van Lipzig, N. P. M.: Clouds enhance Greenland ice sheet meltwater runoff, Nat. Commun., 7, 10266, doi:10.1038/ncomms10266, 2016.

10 Wang, Z.: B-CLDCLASS-LIDAR Interface Control Document, [online] Available from: http://cswww.cira.colostate.edu/icd_pdf.php?avid=36&pvids=12 (Accessed 11 August 2016), 2013.

Zamora, L. M., Kahn, R. A., Eckhardt, S., McComiskey, A., Sawamura, P., Moore, R. and Stohl, A.: Aerosol indirect effects on the nighttime Arctic Ocean surface from thin, predominantly liquid clouds, Atmos Chem Phys, 17(12), 7311–7332, doi:10.5194/acp-17-7311-2017, 2017.

15 Zhao, B., Liou, K.-N., Gu, Y., Jiang, J. H., Li, Q., Fu, R., Huang, L., Liu, X., Shi, X., Su, H. and He, C.: Impact of aerosols on ice crystal size, Atmos Chem Phys, 18(2), 1065–1078, doi:10.5194/acp-18-1065-2018, 2018.

Zib, B. J., Dong, X., Xi, B. and Kennedy, A.: Evaluation and Intercomparison of Cloud Fraction and Radiative Fluxes in Recent Reanalyses over the Arctic Using BSRN Surface Observations, J. Clim., 25(7), 2291–2305, doi:10.1175/JCLI-D-11-00147.1, 2012.
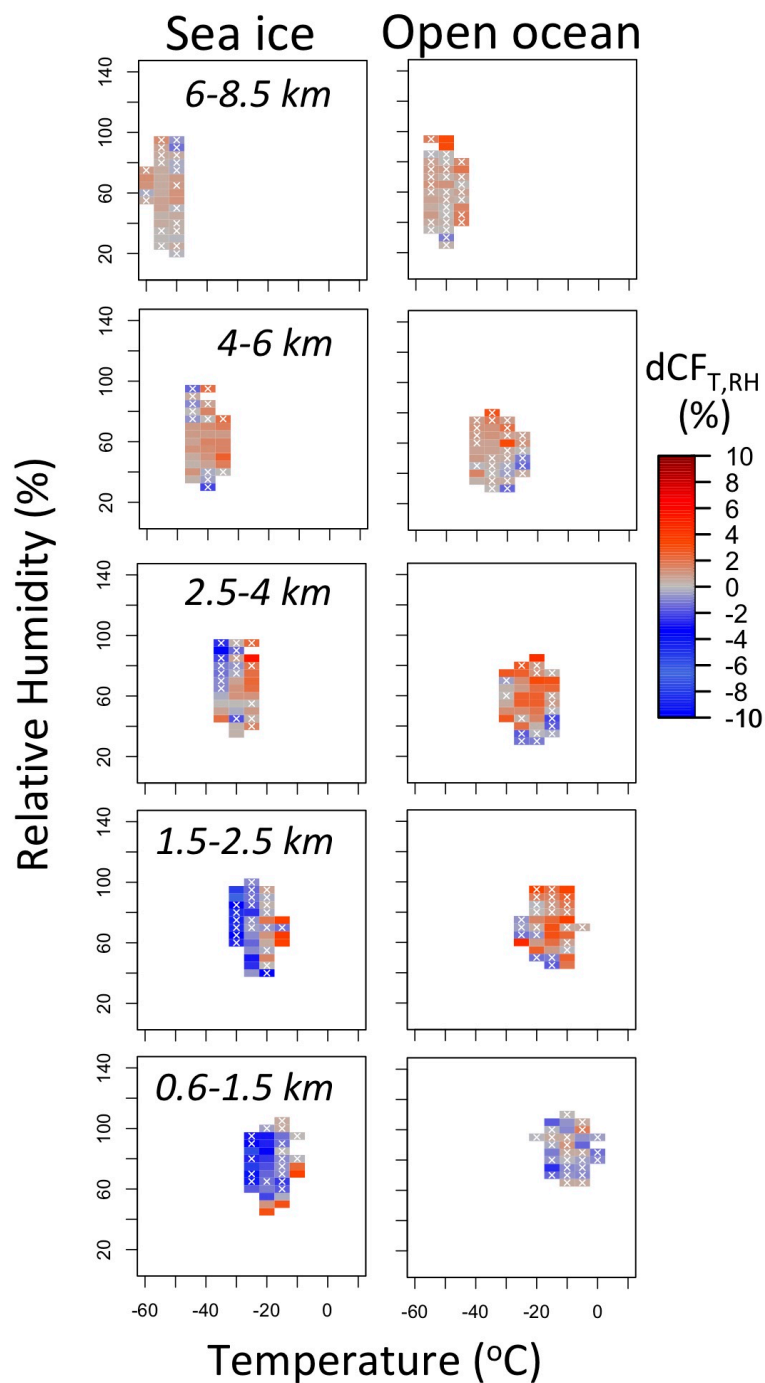
Figure 1: An example of dCF$_{T,RH}$ output at each altitude level. For illustration purposes, here each grid cell represents ≥ 7500 km^2 of gridded observations. Blue and red colors indicate negative and positive dCF$_{T,RH}$, respectively. A white X indicates that the cell value is not significantly different from zero (Wilcoxon rank test, p < 0.05). In all panels, individually significant cells numbered more than expected at random (binomial test, p < 0.001).
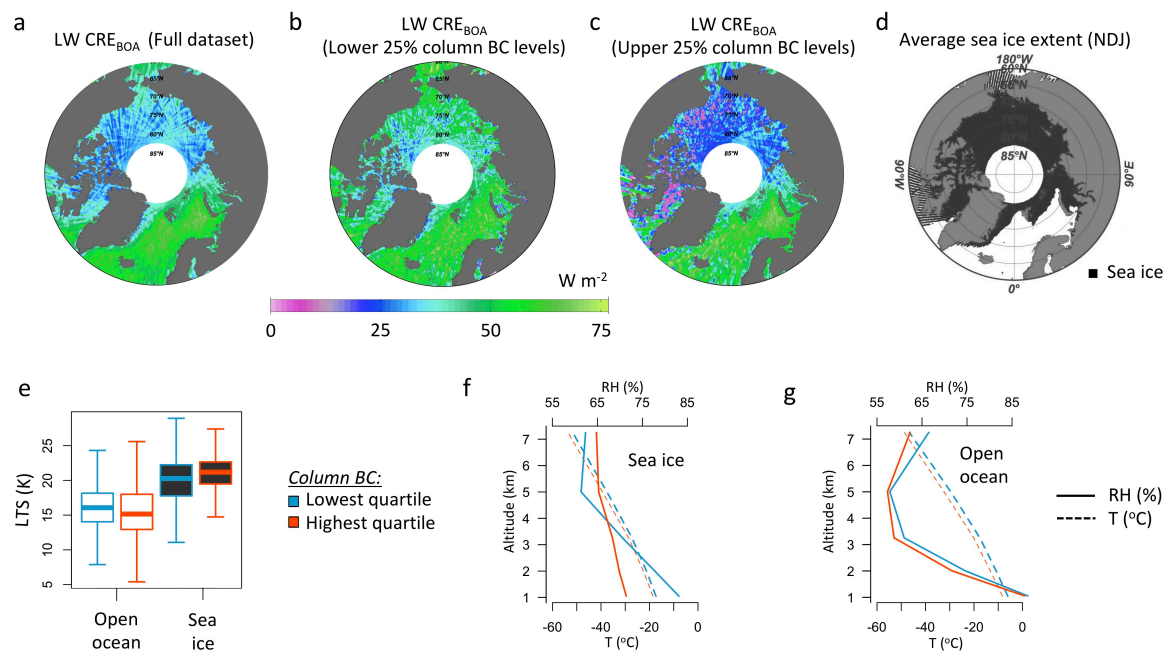
Figure 2: a-c) CloudSat FLXHR-LIDAR longwave cloud radiative effect at the bottom of atmosphere (i.e., surface) (LW CRE$_{BOA}$)
during polar night for a) the full dataset, and the subsets of data containing the lower (b) and upper (c) quartiles of modeled
column BC concentrations. For reference, d) shows the average winter (November to January) sea ice extent up to 82°N. Also
shown are e) boxplots of the lower tropospheric stability (LTS, K), and f, g) the median temperature (T, °C) and relative humidity
(RH, %) for the lower (blue) and upper (red) quartile column BC concentrations over open ocean and sea ice. All differences in e-
g) are significant (p < 0.0001), based on a Wilcoxon rank test.
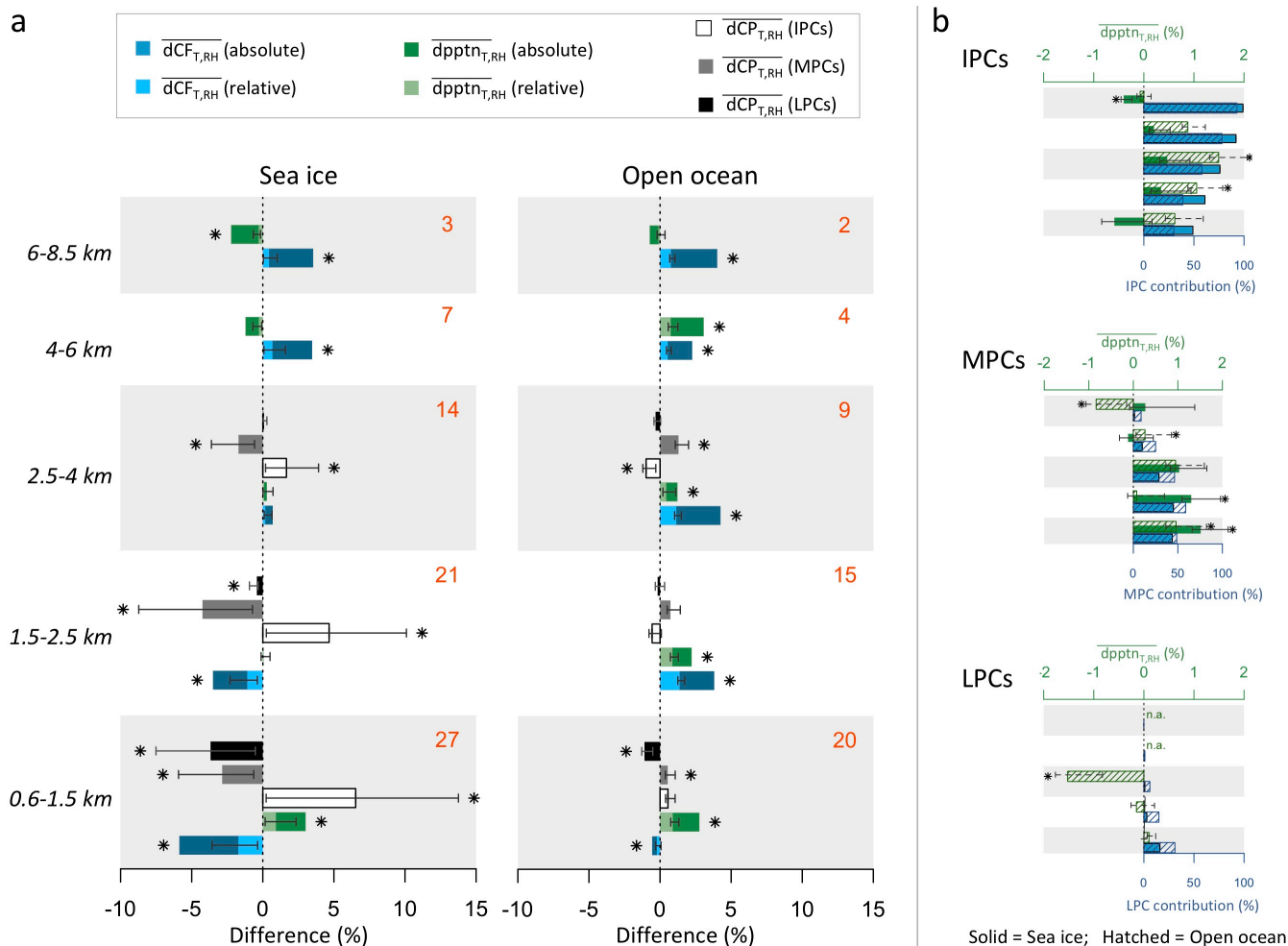
Figure 3: Shown in a) are $\overline{dCF_{T,RH}}$ and $\overline{dpptn_{T,RH}}$ (%) and $\overline{dCP_{T,RH}}$ (up to 4 km, %) in different altitude ranges over sea ice and open ocean. $\overline{dCF_{T,RH}}$ and $\overline{dpptn_{T,RH}}$ data are not stacked, and are presented as both the absolute change within the air volume of interest (darker colors) and the relative percent change with respect to the value found in clean conditions (lighter colors). The $\overline{dBC_{T,RH}}$ values (ng m^{-3}) are presented for each altitude (red, upper right). Shown in b) are the absolute changes in $\overline{dpptn_{T,RH}}$ (green) and the CP distribution (blue) for IPCs, MPCs, and LPCs over sea ice (solid) and open ocean (hatched) at the same altitude ranges as in a). An asterisk (*) indicates that the differences between all and clean conditions were significant, based on a paired Wilcoxon rank test, p > 0.05, using T-RH grid cells containing > 800 (400 for $\overline{dCP_{T,RH}}$) 12.5-km^2 gridded observations. Error bars show bootstrapped 95% confidence intervals for the weighted mean. The same data are presented tabulary in Table S2.
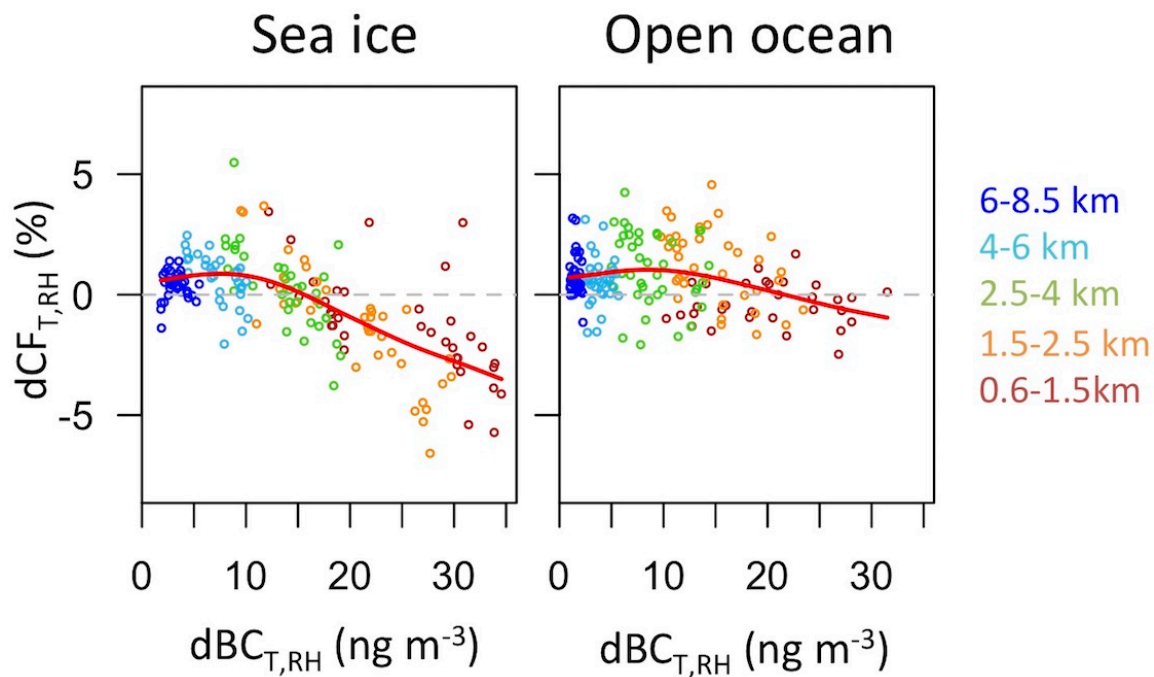
Figure 4: The relationship between dCF$_{T,RH}$ (%) and dBC$_{T,RH}$ (ng m^{-3}) over sea ice and open ocean at different altitude levels (color coded). The red line is a cubic smoothing spline of the data among all altitudes.